ACS APPLIED MATERIALS & INTERFACES

Letter

www.acsami.org

Tunable Water Adhesion on Titanium Oxide Surfaces with Different Surface Structures

Junfei Ou,*[,†] Weihua Hu,[†] Changquan Li,[†] Ying Wang,[‡] Mingshan Xue,[†] Fajun Wang,[†] and Wen Li*[,†]

[†]School of Materials Science and Engineering, Nanchang Hangkong University, Nanchang 330063, People's Republic of China

[‡]Jiangsu Key Laboratory for Solar Cell Materials and Technology, Changzhou 213164, People's Republic of China

ABSTRACT: Tunable water adhesion with high static contact angle (SCA) on titanium oxide surfaces was achieved by a two-step process: first, titanium oxide surfaces with different structures were obtained by immersion the titanium alloy substrates into $H_2O-H_2O_2-HF$ solution at 140 °C for different time of 30, 60, and 120 min; then, low-surface-energy molecules of 1H, 1H, 2H, 2H-perfluorooctyltrichlorosilane (PFOTS) were deposited thereon. SCA for all so-fabricated samples were higher than 150° and sliding angle (SA) for different immersion time of 30 min, 60 min, and 120 min is 180°, 31±2°, and 8±1°, respectively. To analyze the correlation between the surface structures and the dynamic wetting behaviors, we adopted, three contact modes (i.e., Wenzel, Cassie impregnating, and Cassie modes). The analyses showed that the surface adhesion was influenced greatly by water/solid interfacial interaction and could be artificially tuned between Wenzel state with high adhesion to Cassie state with low adhesion through the design of appropriate microstructures.

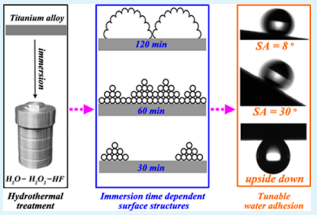

KEYWORDS: *dynamic wetting, sliding angle, contact angle hysteresis, surface structures, titanium oxide, hydrothermal treatment*

1. INTRODUCTION

Materials with special wettability are of great importance in fundamental researches and practical applications.[1−5] Currently, the most studied special wettability is the so-called "superhydrophobicity", which is a term to describe a surface with high static contact angle (SCA, >150°) and low sliding angle (SA, <10°). However, recently, surface with both high SCA and high SA (herein, such surface is denoted as HSSA) has also attracted a great deal of interest,[6,7] which is quite different from superhydrophobic surface (SHS) in the respect of dynamic wetting behaviors. Specifically, water droplets do not stably remain but spontaneously roll off on SHS,[8−10] whereas for HSSA, the extreme case is that the water droplets can pin on the surface even when upside down.[6,7,11] It is believed that the tunable water adhesion (reflected by different SA values) allows the manipulation of water droplets. In other words, if SHS and HSSA samples are arranged together, the droplets will roll off from SHS and stick to HSSA. Such manipulation of water droplet is expected to find wide potential applications in open microdroplet devices with respect to increasing the need for controlled transport of small volumes of liquids in localized chemical reactions, biochemical separation, bio/chem analysis assay, etc.[12−14]

The above mentioned two kinds of special wettability, i.e., SHS and HSSA, are usually inspired by different biological organisms. For instance, the self-cleaning lotus leaf is the typical example of SHS;[15] while the rose petals are examples of HSSA.[6,7] So, "lotus-effect"/"petal effect" are proposed to define these two wetting phenomena, respectively.[3] To reveal the origin of such wetting behaviors, further research was done and revealed that the special surface structures are key factors. Specifically, the protruding nubs about 20−40 μm apart each covered with a nano-scale roughness of epicuticular wax crystalloids are the origin of the superhydrophobicity and self-cleaing properties for lotus leaf.[16] For the rose petal, similar roughness on multiple scales is also observed; however, both of which are larger than that of lotus leaf.[7] This suggests that the larger scale grooves that water droplets can enter into, wetting out and cling is the key factor for the high adhesion of the petal surface.[7]

Inspired by the above mentioned correlation between surface structure and dynamic wetting behaviors, herein, we tune the water adhesion on titanium oxide surface by controlling the surface structures. Specifically, three types of microstructures have been fabricated on the surface of titanium alloy substrates by a simple solution-immersion process; then, the substrate is modified with low-surface-energy molecules. The so-fabricated titanium oxide films show high contrast water adhesion ranging from extremely low to very high. To find out the possible mechanism for such phenomenon, different contact modes (i.e., Wenzel, Cassie impregnating, and Cassie modes) were used. It was supposed that the water/solid contact area decreased as the contact mode changing from Wenzel to Cassie impregnating to Cassie. In this work, such tunable water adhesion and further theoretic mode analyses may offer us an insight into how to control the dynamic wetting behaviors (reflected by SA and contact angle hystersis, CAH) on surfaces with similar static behaviors (reflected by SCA).

2. EXPERIMENTAL SECTION

2.1. Materials and Reagents. Ti alloy (TC4) was obtained from Northwest Institute of Non-ferrous Metal Company, China.

Received: September 11, 2012
Accepted: October 17, 2012
Published: October 17, 2012

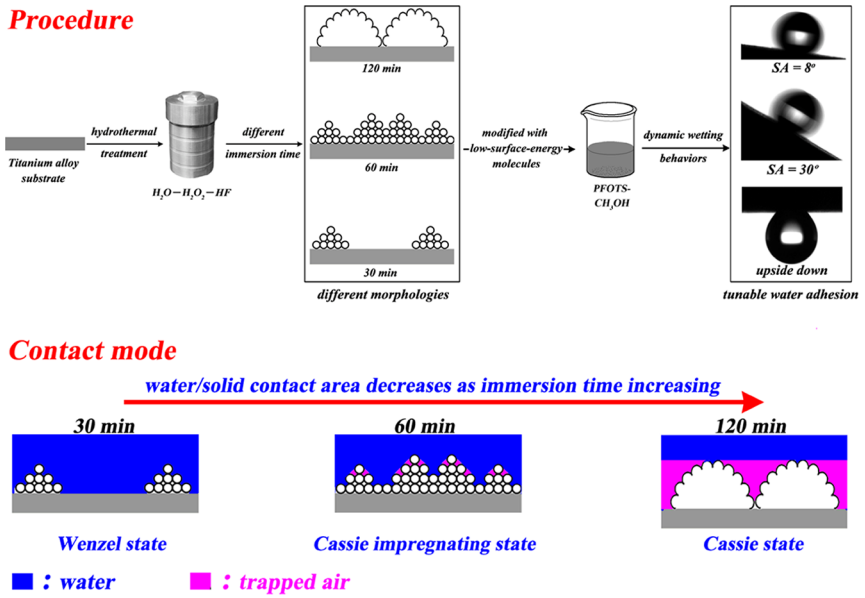

Figure 1. Preparation procedure of surfaces with tunable water adhesion and possible contact modes to explain the tunable water adhesion.

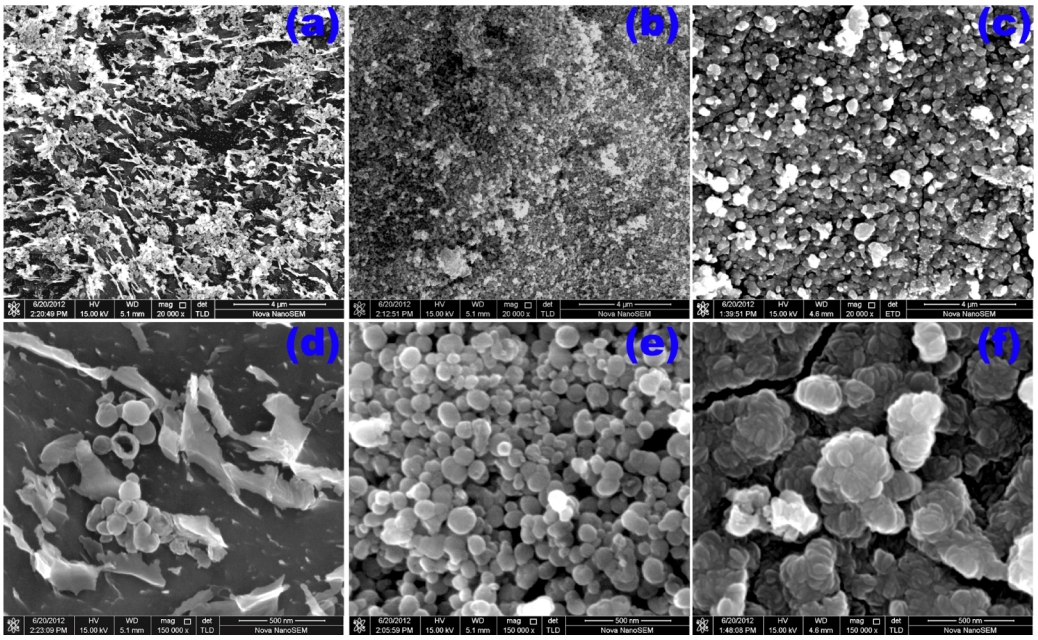

Figure 2. FESEM images of (a, d) *HT* (30), (b, e) *HT* (60), and (c, f) *HT* (120).

1H,1H,2H,2H-Perfluorooctyltrichlorosilane (PFOTS) was purchased from Sigma-Aldrich. Other reagents (HF, H_2O_2, and other solvents) are analytical grade and used as received. Ultrapure water with a resistivity greater than 18.0 MΩ cm was used.

2.2. Preparation of surfaces with Tunable Water Adhesion. Titanium oxide with different surface structures was prepared as follows. Typically, the titanium alloy substrate was firstly ground with abrasive paper (600 and 1200 Cw), and ultrasonicated in acetone, ethanol, and ultrapure water for 10 min, respectively, to get rid of surface contamination. Then, the titanium alloy substrate was transferred into a Teflon vessel with a 100 mL capacity containing H_2O (10 mL) / H_2O_2 (10 ml) / HF (1 ml) hydrothermal solution. The autoclave was maintained at 140 °C for a certain period of time (30, 60, or 120 min), and then cooled down to room temperature. The titanium alloy substrate was taken out and rinsed with ultrapure water and dried in air. Finally, the hydrothermal treated substrate was dipped into PFOTS methanol solution for a period of 1 h and dried at 140 °C for 1h in order to self-assemble a monolayer of low-surface-energy material. The whole process is illustrated in Figure 1. The hydrothermal treated sample by x min and further grafted with PFOTS was coded as HT (x) and HT (x)-F, respectively.

2.3. Characterizations. The surface structures were examined by field emission scanning electron microscopy (FESEM, Nova Nano-SEM, FEI, USA). The phase structures of the as-prepared sample were characterized by an X-ray diffraction (XRD, Bruker-axs's D8AD-VANCE, Germany) equipped with graphite monochromatized Cu K α radiation. The chemical composition of the as-prepared surface was investigated using X-ray photoelectron spectroscopy (XPS), which was conducted on a PHI-5702 electron spectrometer (Physical Electronics, USA) using the Al Kα line as the excitation source with the reference of C 1s at 284.80 eV. The static contact angle (SCA) and sliding angle (SA) were measured with a Krüss DSA20 apparatus at ambient temperature. The volume of the individual water droplet in all measurements was 7 μL. The average SCA and SA values were

dx.doi.org/10.1021/am301946t | ACS Appl. Mater. Interfaces 2012, 4, 5737−5741

obtained by measuring the same sample at least in five different positions. Advancing and receding contact angles (denoted as θ_A and θ_R, respectively) were measured by increasing and decreasing the droplet volume, respectively. The acidity of different solution was detected on a pH meter (Mettler Toledo, FiveEasy) at room temperature (30 °C).

3. RESULTS AND DISCUSSION

Under the hydrothermal conditions, titanium alloy substrate is supposed to react with the hydrothermal solution of H_2O/H_2O_2 / HF by the following chemical reaction equations

$$TiO_2 + 6HF \rightarrow H_2TiF_6 + 2H_2O \quad (1)$$

$$Ti + 6HF \rightarrow H_2TiF_6 + 2H_2\uparrow \quad (2)$$

$$Ti + 2H_2O_2 \rightarrow TiO_2 + 2H_2O \quad (3)$$

HF can remove the TiO_2 layer that may be formed during the abrasion and ultrasonication process on the substrate (eq 1). After removing the expected and useless TiO_2 layer, HF may further react with the titanium species on the substrate, just as shown in eq 2. Thus, a freshly-prepared titanium alloy substrate with no oxide layer was directly exposed to the hydrothermal solution. Then, the titanium species are supposed to react with H_2O_2, another important component of the hydrothermal solution, to form a titanium oxide layer.

At different stages of the hydrothermal treatment, the main reactions are supposed to be different, which may further account for the different surface structures of *HT* (*x*) samples. Specifically, the main reactions at early stage are dissolution of Ti or TiO_2, which may be formed in the process of pretreatment or hydrothermal treatment (oxidation of titanium species); so, the deposition and growth of TiO_2 may be suppressed by eq 1. Consequently, sparsely-distributed nano-ribbons and nano-spheres (diameter of 70−140 nm) are observed on the surface of *HT* (30) (Figure 2a, d). As the immersion time prolonging to 60 min, due to the consumption of HF, the dissolution of TiO_2 becomes much lower and, correspondingly, the deposition/growth of TiO_2 is enhanced. So, the surface of *HT* (60) was densely covered by nano-spheres (Figure 2b) and the size of which remain almost unchanged as compared *HT* (*60*) with *HT* (*30*) (Figure 2d) and Figure 2e). Further increasing the hydrothermal treating time to 120 min, nan-spheres integrate to form micro- (∼ 1 μm) or submicro-particles (∼200 nm) (Figure 2c, f). This integration may be attributed to the acidity variation of the hydrothermal solution. Specifically, for a short hydrothermal treating time of 30 or 60 min, pH value of the hydrothermal solution was still in a high level (Table 1); so, the dissolution of titanium oxide (eq 1) nanospheres can not be neglected. In other words, the integration of such no-spheres was suppressed greatly due to the dissolution of the as-deposited titanium oxide. However, as the hydrothermal treating time prolonging to 120 min, pH of hydrothermal solution became much higher (pH 2.42, Table 1) and the rate of dissolution of titanium oxide nano-spheres was expected to be much lower; so, the nanospheres tend to grow and integrate to form micro- or submicro-particles. Moreover, cracks with a width of ∼50 nm were formed [Figure 2f]. Similar crack-forming phenomenon has been widely observed for the deposition of titanium oxide film on different substrates by different methods and it is believed that this can be ascribed to the shrinkage during post drying process.[22,23]

Table 1. Variation in pH Value for Hydrothermal Solution As a Function of Hydrothermal Treating Time

time (min)	0	30	60	120
pH	1.67 ± 0.05	1.82 ± 0.07	1.96 ± 0.06	2.42 ± 0.07

To ascertain the above mentioned chemical reactions, XRD and XPS analyses (Figure 3) were performed to monitor the variation of surface species. However, XRD results showed that there was no new peak emerged as compared the XRD pattern of *HT* (120) (Figure 3a-i) with HF etched titanium alloy substrate (coded as *HE*, Figure 3a-ii). This suggests that the so-formed film by hydrothermal treatment were amorphous. XPS Ti 2p spectra of *HE* and *HT* (120) were also provided and compared (Figure 3b). Signals located at 454.1 eV and 458.8 eV were observed for *HE* and *HT* (120), respectively. The former one is a typical value of Ti (0) metal,[17,18] whereas the latter value with higher binding energy is very similar with the reported ones of TiO_2.[19−21] So, it is deduced that a layer of TiO_2 has been generated under the oxidation of H_2O_2, just as shown in eq 3.

To characterize the wetting behaviors of water on surface, a droplet is placed thereon. Due to the heterogeneity of *HT-F* surfaces, the droplet will come to rest at a local energy minimum and there will be an energy barrier for any advancing or receding of the water droplet on the surface. Such kinetic barrier difference in the advancing and receding modes gives rise to contact angle hysteresis (CAH = $\theta_{adv} - \theta_{rec}$), leading to the adhesive force. So, it is believed that water adhesion on surfaces can be reflected by CAH. Another important parameter to reflect the dynamic wetting behavior is SA, which is the critical tilt angle when the droplet sliding on a tilted surface. As summarized in Table 2, the *HT-F* samples show high contrast CAH/SA values. Specifically, with the increase of immersion time from 30 min to 60 min and finally to 120 min, SA/CAH decreases from 180° (the water droplet is firmly pinned on the surface even when the upside down)/60° to 31 ± 2°/33° and then to 8 ± 1°/9°, respectively. Such variation of SA/CAH values suggests that the surface adhesion on *HT-F* is quite different. It is believed that the surface adhesion (F_{ad}) is a product of water/solid interfacial interaction (denoted as *I*) and contact area (denoted as *A*)

$$F_{ad} = kIA \quad (4)$$

$$F_{ad} \propto A \quad (5)$$

where *k* is a constant and *I* is closely related with the solid chemical nature, which is supposed to be the same for the three samples in the present study because the surfaces are all modified with PFOTS. So, eq 4 can be simplified to eq 5. In other words, the surface adhesion F_{ad} is in proportion to contact area *A*.

To analyze the water/solid contact area, three distinct contact modes (Wenzel,[24] Cassie[25] and Cassie impregnating mode[15,26]) were adopted. For *HT* (30)-*F*, the surface is characterized by big gaps between neighbor rough micro-structures; so, water tends to penetrate into the grooves and the contact mode of Wenzel state is obtained (Figure 1). In this situation, the water/solid contact area is largest and the water/solid interfacial interaction is expected to be highest; so, the water droplet can be firmly attached to the surface. In contrast, for *HT* (120)-*F*, the surface is characterized by hierarchical miro- and nano-structures, which is widely accepted as a

dx.doi.org/10.1021/am301946t | ACS Appl. Mater. Interfaces 2012, 4, 5737−5741

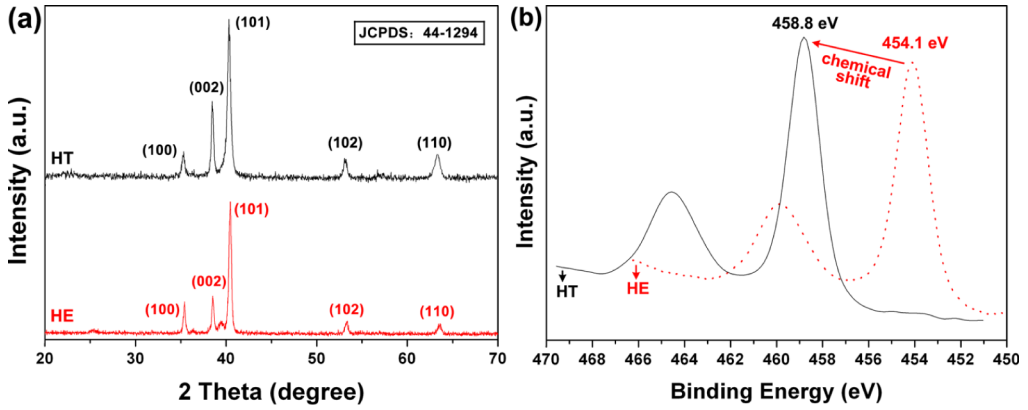

Figure 3. (a) XRD patterns and (b) XPS spectra of different samples. HE and HT denote HF etched and hydrothermal treated samples, respectively.

Table 2. Wetting Behaviors of Water on Different Samples

item	SCA (deg)	θ_{adv} (deg)	θ_{rec} (deg)	CAH (deg)	SA (deg)
HT (30)-*F*	153 ± 2	161 ± 3	101 ± 2	60	180
HT (60)-*F*	158 ± 1	163 ± 2	130 ± 2	33	31±2
HT (120)-*F*	160 ± 1	164 ± 2	155 ± 2	9	8±1

prerequisite for Cassie state. In this state, water/solid contact area fraction f_1 can be calculated from the following equation[25]

$$\cos\theta = f_1\cos\theta - (1 - f_1) \quad (6)$$

where θ is the SCA (= 160 ± 1°) and θ_1 is intrinsic CA (= 120°). The calculated f_1 is in the range from 0.1090 to 0.1328. So, water droplet is suspended by the gas layer trapped at the microscales (Figure 1); thus, the surface adhesion is extremely low due to the low water/solid contact area. Another contact mode, Cassie impregnating state,[15,26] is proposed to analyze the sample of *HT* (60)-*F*. The feature of this contact mode is that the grooves of the solid are wetted with water and solid plateaus are dry (Figure 1); consequently, the adhesion of the surface is between that of the above two states (i.e., Wenzel and Cassie state) and the water droplet rolls off with the surface significantly tilted (herein, SA= 31 ± 2°, as shown in Table 1).

Another obvious difference among *HT-F* samples on wetting behaviors are SCA values; just as summarized in Table 2, the SCA increases as the hydrothermal treating time prolonging. This may also be attributed to the different surface structures for these samples. In other words, as the immersion time increases from 30 min to 60 min and finally to 120 min, the surface features changes from nano-structures to micro/nanostructures, the latter of which is supposed to be a key parameter for superhydrophobicity and high SCA.

4. CONCLUSIONS

In summary, tunable water adhesion on titanium oxide surface with high SCA have been achieved by controlling the surface structures. It is believed that such structure-dependent water adhesion (F_{ad}) is in proportion to the water/solid contact area (A), which decreases as hydrothermal treating time prolonging from 30 min (Wenzel contact mode, solid surface is completed wetted by water, i.e., 100 % wetted) to 60 min (Cassie impregnating mode, partially wetted) and finally to 120 min (Cassie mode, ~10 % wetted). Correspondingly, the adhesion force (reflected by SA and CAH) decreases gradually. It is hoped that these results and related theoretical analyses may provide a new strategy and some insights into how to manipulate the dynamic behaviors of surface with high SCA.

AUTHOR INFORMATION

Corresponding Author

*E-mail: wenl@ualberta.ca; oujunfei_1982@163.com.

Notes

The authors declare no competing financial interest.

ACKNOWLEDGMENTS

The authors acknowledge with pleasure the financial support of this work by the National Natural Science Foundation of China (Grants 21203089 and 51263018), Natural Science Foundation of Jiangxi Province (Grants 2010GZC0164), Key Technology R&D Program (Grants 2010BGB00100) of Jiangxi Province, the International Science and Technology Cooperation Plan of Jiangxi Province (Grants 2010EHA01300), the National Science Foundation of Hangkong (Grants 2010ZE56012), and the Department of Education of Jiangxi Province (Grants GJJ11502; GJJ12422; GJJ12424).

REFERENCES

(1) Nosonovsky, M. *Nature* **2011**, *477*, 412.
(2) Wong, T.; Kang, S. H.; Tang, S. K. Y.; Smythe, E. J.; Hatton, B. D.; Grinthal, A.; Aizenberg, J. *Nature* **2011**, *477*, 443.
(3) Liu, K.; Yao, X.; Jiang, L. *Chem. Soc. Rev.* **2010**, *39*, 3240.
(4) Zhang, Y.; Chen, Y.; Shi, L.; Li, J.; Guo, Z. *J. Mater. Chem.* **2012**, *22*, 799.
(5) Liu, M.; Zheng, Y.; Zhai, J.; Jiang, L. *Acc. Chem. Res.* **2010**, *43*, 368.
(6) Liu, K.; Du, J.; Wu, J.; Jiang, L. *Nanoscale* **2012**, *4*, 768.
(7) Feng, L.; Zhang, Y.; Xi, J.; Zhu, Y.; Wang, N.; Xia, F.; Jiang, L. *Langmuir* **2008**, *24*, 4114.
(8) Nosonovsky, M.; Bhushan, B. *Nano Lett.* **2007**, *7*, 2633.
(9) Koch, K.; Bhushan, B.; Barthlott, W. *Soft Matter* **2008**, *4*, 1943.
(10) Bhushan, B.; Jung, Y. C.; Koch, K. *Langmuir* **2009**, *25*, 3240.
(11) Li, J.; Liu, X.; Ye, Y.; Zhou, H.; Chen, J. *J. Phys. Chem. C* **2011**, *115*, 4726.
(12) Winkleman, A.; Gotesman, G.; Yoffe, A.; Naaman, R. *Nano Lett.* **2008**, *8*, 1241.
(13) Dorvee, J. R.; Derfus, A. M.; Bhatia, S. N.; Sailor, M. J. *Nat. Mater.* **2004**, *3*, 896.
(14) Suh, K. -Y.; Park, M. C.; Kim, P. *Adv. Funct. Mater.* **2009**, *19*, 2699.
(15) Lafuma, A.; Quéré, D. *Nat. Mater.* **2003**, *2*, 457.
(16) Feng, L.; Li, S.; Li, Y.; Li, H.; Zhang, L.; Zhai, J.; Song, Y.; Liu, B.; Jiang, L.; Zhu, D. *Adv. Mater.* **2002**, *14*, 1857.

(17) Moulder, J.; Stickle, W. F.; Sobol, P. E.; Bomben, K. D. *Handbook of X-ray Photoelectron Spectroscopy*, 2nd ed.; Perkin Elemer Corporation: Eden Prairie, MN, 1992.
(18) Ou, J.; Liu, M.; Li, W.; Wang, F.; Xue, M.; Li, C. *Appl. Surf. Sci.* **2012**, *258*, 4724.
(19) Ou, J.; Wang, J.; Zhang, D.; Liu, S.; Yan, P.; Liu, B.; Yang, S. *Colloids Surf., B Biointerfaces* **2010**, *76*, 123.
(20) Collins, R. J.; Shin, H.; DeGuire, M. R.; Heuer, A. H.; Sukenik, C. N. *Appl. Phys. Lett.* **1996**, *69*, 860.
(21) Zhang, F.; Jin, S.; Mao, Y.; Zheng, Z.; Chen, Y.; Liu, X. *Thin Solid Films* **1997**, *310*, 29.
(22) Ou, J.; Wang, F.; Xue, M.; Wang, Y.; Yao, J.; Li, W. *Chem. Lett.* **2012**, *41*, 669.
(23) Pizem, H.; Sukenik, C. N.; Sampathkumaran, U.; McIlwain, A. K.; De Guire, M. R. *Chem. Mater.* **2002**, *14*, 2476.
(24) Wenzel, R. N. *Ind. Eng. Chem.* **1936**, *28*, 988.
(25) Cassie, A. B. D.; Baxter, S. *Trans. Faraday Soc.* **1944**, *40*, 546.
(26) Bormashenko, E.; Pogreb, R.; Stein, T.; Whyman, G.; Erlich, M.; Musin, A.; Machavariani, V.; Aurbach, D. *Phys. Chem. Chem. Phys.* **2008**, *10*, 4056.